Dalton Transactions

ROYAL SOCIETY OF CHEMISTRY

COMMUNICATION

View Article Online
View Journal | View Issue



Cite this: *Dalton Trans.*, 2025, **54**, 11801

Received 9th May 2025,
Accepted 26th June 2025

DOI: 10.1039/d5dt01103e

rsc.li/dalton



# Evaluating a triaza-18-crown-6 picolinate chelator for [$^{212/203}$Pb]$Pb^{2+}$ and [$^{212/213}$Bi]$Bi^{3+}$ theranostics†

Desiree Fiaccabrino,[a,b] Tinotenda Masvikeni,[a] Brooke L. McNeil,[b,c] Brian O. Patrick,[d] María de Guadalupe Jaraquemada-Peláez,*[e] Paul Schaffer *[b,c,f] and Chris Orvig *[a]

**$H_3$tripa ($H_3$macrotripa), a triaza-18-crown-6 macrocycle bearing three picolinate arms, enables quantitative radiolabeling of [$^{203}$Pb]$Pb^{2+}$ and [$^{213}$Bi]$Bi^{3+}$ and exhibits robust human serum stability. NMR spectroscopy, X-ray crystallography, density functional theory, and UV-potentiometry investigate its coordination geometry and thermodynamics with $Bi^{3+}$ and $Pb^{2+}$, highlighting $H_3$tripa as a promising Pb/Bi theranostic chelator.**

Targeted alpha therapy (TAT) has emerged as a promising approach in oncology, leveraging the high linear energy transfer (LET) of alpha particles to induce localized and irreparable DNA damage in cancer cells. Among the alpha-emitting radioisotopes currently under investigation, $^{213}$Bi has garnered significant attention due to its relatively short half-life (45.6 min) and high LET, making it effective for targeting small tumours or micrometastases.[1,2] While the parent radionuclide, $^{225}$Ac, is better matched to large, slow-clearing biomolecules due to its extended half-life (9.92 d), the shorter half-life of $^{213}$Bi aligns better with the pharmacokinetics of small targeting agents.[3] In addition to its therapeutic capabilities, $^{213}$Bi emits a gamma photon (440 keV), enabling SPECT imaging that facilitates real-time monitoring of the radiopharmaceutical distribution and personalized dose adjustment.[4,5] Despite these advantages, the short half-life of $^{213}$Bi poses logistical challenges in production, distribution, and administration.[6] To mitigate these issues, researchers are exploring an *in vivo* generator based on $^{212}$Pb (10.64 h, $\beta^-$), which decays to $^{212}$Bi (60.55 min, α). The longer half-life of $^{212}$Pb allows for more flexible handling and extended accumulation at tumour sites.[6] Moreover, the combination of $^{203}$Pb (51.8 h, γ) for SPECT imaging and $^{212}$Pb/$^{212}$Bi for therapy constitutes a powerful theranostic pair, enabling both treatment and monitoring within the same framework.

The effectiveness of Pb/Bi-based radiopharmaceuticals inherently depends on the chelators used to stably bind these radionuclides (Fig. 1). Established chelators, such as $H_4$DOTA and TCMC, while valuable, may not fully retain $^{212}$Bi after the decay of $^{212}$Pb due to internal conversion events that can lead to dissociation of the daughter nuclide. This phenomenon presents a major challenge in designing chelators for *in vivo*

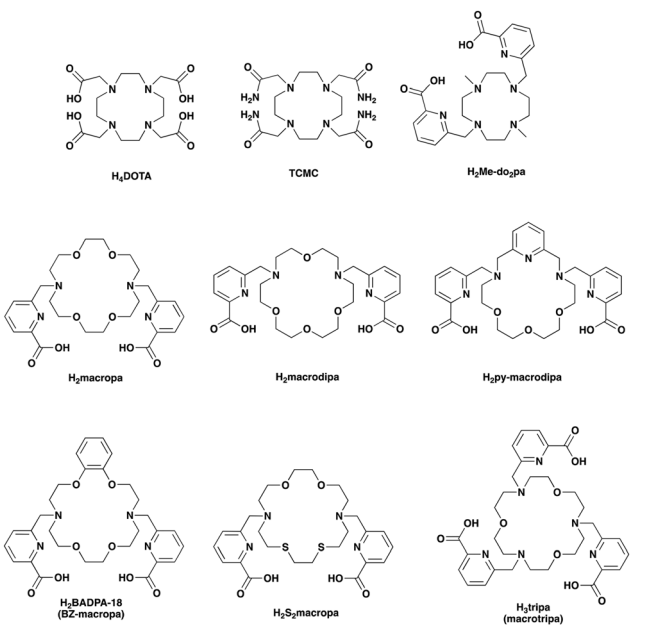


**Fig. 1** Chemical structures of discussed chelators for $Pb^{2+}$ and $Bi^{3+}$.

[a]*Medicinal Inorganic Chemistry Group, Department of Chemistry, University of British Columbia, 2036 Main Mall, Vancouver, British Columbia V6T 1Z1, Canada. E-mail: orvig@chem.ubc.ca*
[b]*Life Sciences Division, TRIUMF, 4004 Wesbrook Mall, Vancouver, British Columbia, V6T 2A3, Canada*
[c]*Department of Chemistry, Simon Fraser University, 8888 University Drive, Burnaby, V5A 1S6, Canada*
[d]*Department of Chemistry, University of British Columbia, 2036 Main Mall, Vancouver, British Columbia V6T 1Z1, Canada*
[e]*Department of Molecular Oncology, BC Cancer Research Institute, Vancouver, BC V5Z1L3, Canada*
[f]*Department of Radiology, University of British Columbia, Vancouver, British Columbia V5Z 1M9, Canada*

†Electronic supplementary information (ESI) available: Experimental section, additional data, figures and tables. See DOI: https://doi.org/10.1039/d5dt01103e

$^{212}$Pb/$^{212}$Bi generators.[7,8] New classes of chelators, including diaza-crown ethers appended with picolinic acid groups, have shown promise in improving binding affinity and radiolabeling efficiency, although further studies are needed to understand their *in vivo* performances.[9–12]

We investigated a triaza-18-crown-6 macrocycle featuring three picolinate arms (first reported[13] by Hu *et al.* as $H_3$macrotripa while this work was just beginning) for its dual size-selectivity within the lanthanoid series, and designated it $H_3$tripa. This study presents the first radiopharmaceutical evaluation of $H_3$tripa with [$^{203}$Pb]$Pb^{2+}$ and [$^{213}$Bi]$Bi^{3+}$, employing NMR spectroscopy, X-ray crystallography, and density functional theory (DFT) to investigate coordination geometries, and UV-potentiometry to determine protonation and formation constants with $Pb^{2+}$ and $Bi^{3+}$.

The coordination properties of $H_3$tripa were explored by forming binary metal complexes with $Pb^{2+}$ and $Bi^{3+}$. Equimolar amounts of the ligand were reacted with corresponding metal salts in $D_2O$ and pD was adjusted to 6–7 using 0.5 M NaOD. Spectral changes were observed using NMR spectroscopy ($^1$H and $^1$H–$^1$H COSY) and further confirmed using high-resolution electrospray ionization mass spectrometry (HR-ESI-MS), in which the expected $[M + H]^+$ species verified metal coordination.

The $^1$H NMR spectrum of the $Bi^{3+}$ complex (Fig. 2A) exhibits well-defined, sharp peaks, indicating a rigid conformation environment with no fluctuation around the metal. Furthermore, the complex presents the characteristic diastereotopic splitting consistent with chirality generation upon binding to a metal centre, thus confirming metal ion complexation. The spectrum of $[Bi(Htripa)]^+$ shows the formation of an asymmetric complex in solution, as indicated by three inequivalent proton signals in the aromatic region that correspond to three picolinic acid arms binding in distinct environments. More specifically, two arms (A and B) give a set of overlapping signals, namely a triplet at $\delta$ 8.36 ppm (2H) and a broad multiplet at $\delta$ 8.13–8.04 ppm (4H), whereas the third arm (C) produces a separate set consisting of a triplet at $\delta$ 7.96 ppm (1H) and two doublets at $\delta$ 7.78 ppm (1H) and $\delta$ 7.49 ppm (1H). The methylene hydrogens associated with the picolinic acids give rise to three pairs of doublets as they become inequivalent upon coordination to the metal centre; these are recognisable by their large geminal $J_{H-H'}$ couplings of approximately 15–17 Hz. Although partially obscured in the $^1$H NMR spectrum by the water signal, the doublets are observable in the $^1$H–$^1$H COSY spectrum (Fig. S14†).

In contrast, the $^1$H NMR spectrum for [Pb(Htripa)] reveals a dynamic heterogeneous coordination environment. Multiple broad peaks appear in both the aromatic and aliphatic regions, consistent with metal–ligand species rapidly exchanging. In the aromatic region two sets of picolinate resonances can be identified, a major set (purple asterisks) and a weaker less intense group (red asterisks), suggesting either two rapidly interconverting coordination isomers, with one conformer strongly favored (purple asterisks), or alternatively a single asymmetric species in which the three arms become magnetically non-equivalent. The broad signals in the aliphatic region support the presence of fast exchange phenomena, typically associated with the flexibility of $Pb^{2+}$ complexes attributed to the lone pair activity on $Pb^{2+}$ and its inherent stereochemical lability.[14,15] To probe this fluxional behaviour further, variable temperature (VT) $^1$H NMR measurements were performed 25–90 °C (Fig. 2B). As the temperature was raised to ~55 °C, further broadening of the aliphatic peaks was observed, suggesting increased molecular motion or conformational exchange. Simultaneously, one set of aromatic peaks diminished, likely merging with the predominant species as exchange processes accelerated. At even higher temperatures (75–90 °C), the aromatic signals sharpened, indicating that conformational averaging led to the predominance of a single species with rapid interconversion, although the aliphatic signals remained partially broad. These observations leave open the possibility that the dynamic averaging originates

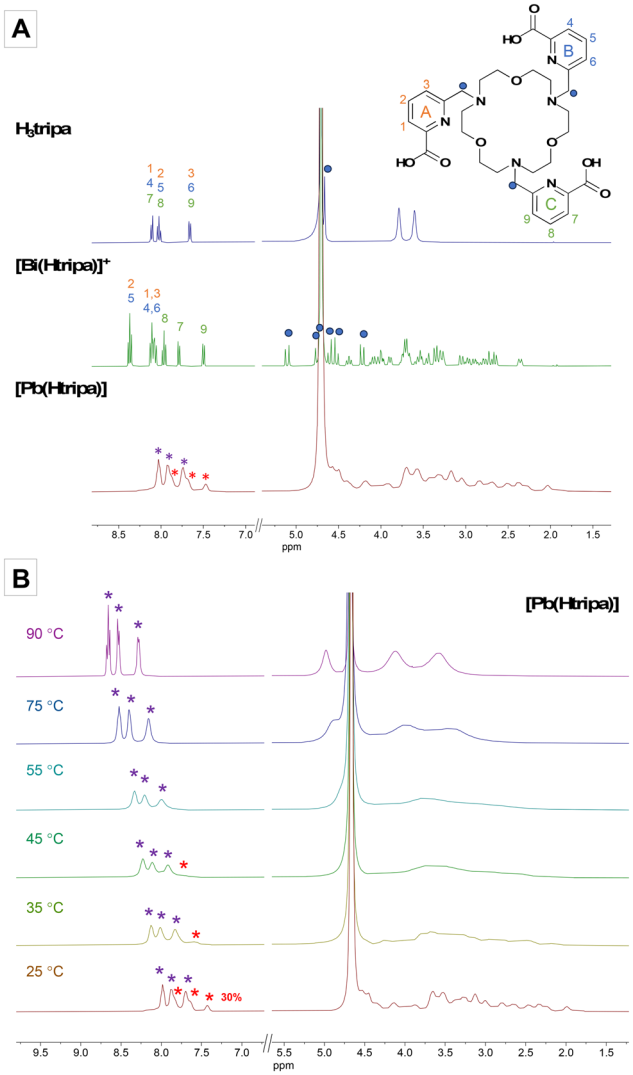


**Fig. 2** (A) $^1$H NMR spectra of $H_3$tripa (400 MHz, $D_2O$, pD 2), $[Bi(Htripa)]^+$ and [Pb(Htripa)] (400 MHz, $D_2O$, pD 6–7). (B) Variable temperature $^1$H NMR spectra of [Pb(Htripa)] (400 MHz, $D_2O$, pD 7).

either from symmetric reorientation within the coordination sphere or from rapid dissociation and recoordination of donor groups. This behaviour is especially relevant, as kinetic inertness is a criterion for radiopharmaceutical applications, and the observed fluxionality might impact the long-term stability of the $Pb^{2+}$ complex.

An X-ray quality crystal of the $Pb^{2+}$ complex with the $H_3$tripa ligand was obtained *via* slow evaporation of water at ambient temperature, yielding irregularly shaped crystals. The molecular structure is bimetallic (Fig. 3).[22]

The $H_3$tripa ligand coordinates one $Pb^{2+}$ ion, designated 'Pb2', through two bidentate picolinic acid groups in a *cis* arrangement – both are positioned on the same side of the metal centre. Additionally, Pb2 is coordinated by five donor atoms from the macrocycle: one oxygen and one nitrogen interact more strongly (Pb–O/N ≤ 2.7 Å), whereas the other three donors form longer interactions (3.1–3.3 Å). The third picolinic acid group coordinates the second $Pb^{2+}$ ion, designated 'Pb1' here, along with two oxygen atoms, and one nitrogen atom from the macrocycle.

The coordination environment around Pb2 likely provides a representation of how $H_3$tripa may bind $Pb^{2+}$, with at least two picolinic acid groups playing a key role in binding. Unfortunately, due to the presence of the second $Pb^{2+}$ ion, further structural insights into the monometallic binary [Pb(tripa)]$^-$ complex *via* crystallography remain limited. Unfortunately, no X-ray quality crystals were obtained for the Bi(tripa) complex.

Given the complexities observed in the NMR and crystallographic data, DFT calculations were conducted to further elucidate the coordination geometries of the [Pb(tripa)]$^-$ and Bi(tripa) complexes. Optimized geometries for both were obtained (Fig. 4), and several conformations explored, including those where all three picolinate arms coordinate from one side of the coordination plane and alternate arrangements in which two arms adopt a *cis* configuration while the third binds more flexibly from the opposite side. In some cases, only two picolinate groups coordinate the metal while the third remains unbound.

The lowest energy conformation for [Pb(tripa)]$^-$, favoured by an energy margin of approximately 20.4 kJ mol$^{-1}$, displays octadentate coordination. In this geometry, two picolinic acid groups bind strongly in a *cis* arrangement, while the third arm extends away from the coordination plane. This arrangement distorts the macrocyclic backbone so that only four out of six donor atoms (two nitrogens and two oxygens) are directly involved in coordination. These trends are consistent with experimental observations seen in related macrocycles based on picolinic acid, where donor atoms tend to coordinate from one side of the metal centre, leading to a hemidirected geometry.[16,17] For the Bi(tripa) complex, the optimized geometry closely mirrors that of the $Pb^{2+}$ complex. On average, the $Bi^{3+}$ complex shows shorter metal–donor bond lengths compared to the $Pb^{2+}$ complex. This contraction arises from both the smaller ionic radius and the higher charge density of $Bi^{3+}$, the latter leading to the chelate having stronger interactions with $Bi^{3+}$; Bi–O bond distances are shorter (approximately 2.28 Å) compared to Pb–O bonds, and similar trends are noted for Bi–N *versus* Pb–N distances.

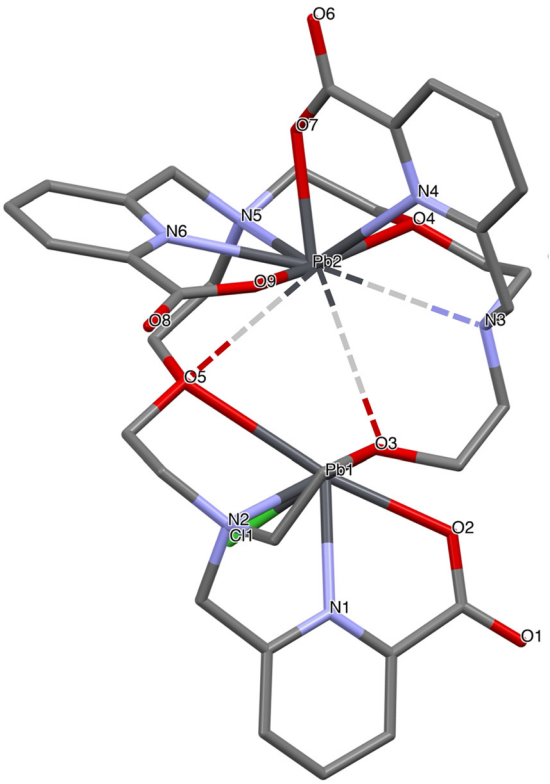


**Fig. 3** Representation of the Cl-bridged dimer $\{[Pb2(tripa)Cl]\}_2$. Only the asymmetric unit, one [Pb2(tripa)Cl] fragment, is shown; the second half is generated by inversion symmetry. Longer interactions (Pb–O/N ≥ 3.1 Å) are represented with dashed lines, hydrogens have been omitted for clarity.

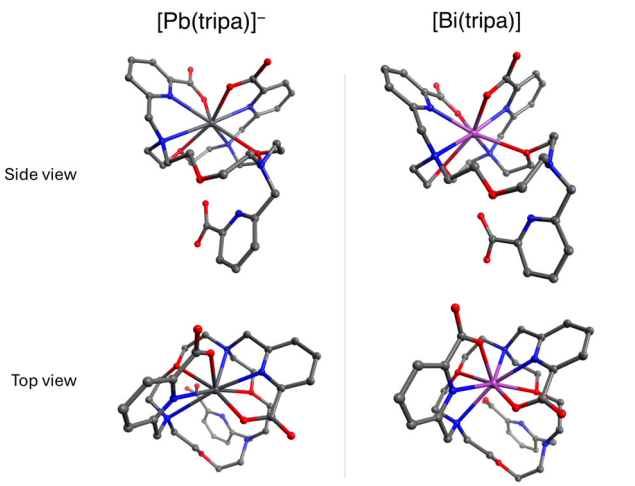


**Fig. 4** DFT-optimized structures of [Pb(tripa)]$^-$ (left) and Bi(tripa) (right). Hydrogen atoms are omitted for clarity.

Combined UV-potentiometric titrations between pH 2 and 11 were used to determine protonation constants for $H_3$tripa, with results consistent with Hu *et al.* (Table S2†),[13] and formation constants for $H_3$tripa with $Pb^{2+}$ and $Bi^{3+}$ (Fig. 5 and Table 1). It was found that $H_3$tripa forms complexes with both metal ions at very low pH; however, the direct evaluation of formation constants under highly acidic conditions was challenging due to the limitations of the potentiometric electrode. To overcome this, in-batch UV-Vis spectrophotometric titrations were undertaken, involving incrementally acidifying preformed complexes. This approach allowed for the complete determination of formation constants for $[Bi(H_2tripa)]^{2+}$ and $[Pb(H_2tripa)]^{+}$.

For the $Bi^{3+}$ complex, the speciation diagram evinces the predominant species to be the neutral Bi(tripa) at pH 7.4, with a minor population of the monoprotonated $[Bi(Htripa)]^{+}$. As pH > 8, the hydroxide-bound species $[Bi(tripa)(OH)]^{-}$ becomes prevalent, verifying that the Bi–ligand interactions are robust even in mildly alkaline media. Conversely, the $Pb^{2+}$ complex exists predominantly as the neutral monoprotonated [Pb(Htripa)] species at physiological pH, with only a small fraction present as the fully deprotonated $[Pb(tripa)]^{-}$. This behaviour suggests that proton competition plays a more significant role for the binding of $Pb^{2+}$ than for $Bi^{3+}$, consistent with the observed higher binding affinity of $H_3$tripa for $Bi^{3+}$.

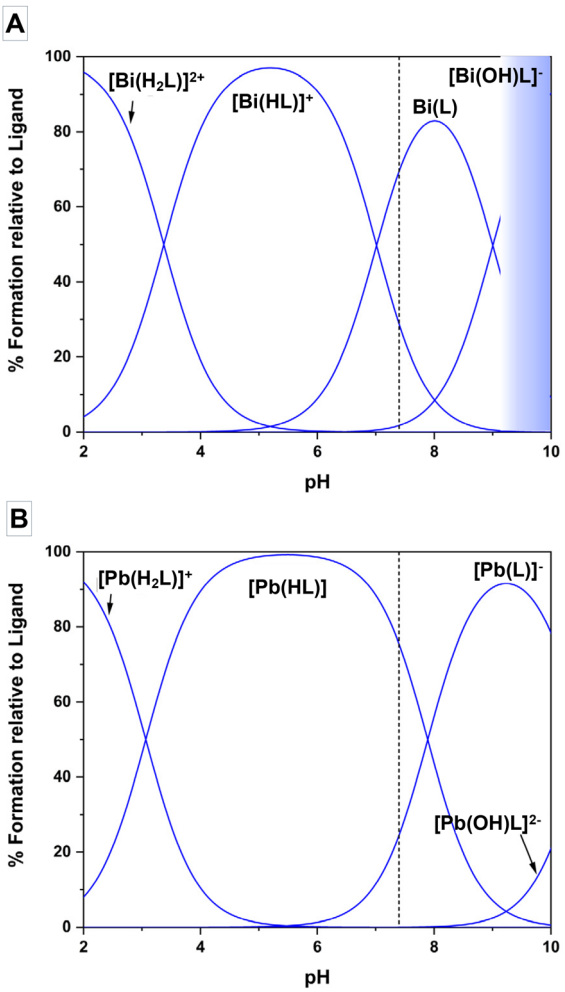


**Fig. 5** Speciation plot for $H_3$tripa with (A) $Bi^{3+}$ and (B) $Pb^{2+}$; dashed line represents pH 7.4. The gradient-filled area of the graph indicates where precipitation occurred, and speciation could not be elucidated.

**Table 1** Stepwise stability constants (log *K*) of $H_3$tripa complexes with $Bi^{3+}$ and $Pb^{2+}$

| Equilibrium reaction | $Bi^{3+}$ | $Pb^{2+}$ |
|---|---|---|
| M + L ⇆ ML | 27.21(4)[a] | 24.75(1)[a] |
| ML + H ⇆ MHL | 7.02(4)[a] | 7.89(2)[a] |
| MHL + H ⇆ $MH_2L$ | 3.37(2)[a,b] | 3.07(2)[a,c] |
| M(OH)L + H ⇆ ML | 9.0(1)[a] | 10.58(4)[a] |

[a] UV-potentiometric titration at $I$ = 0.16 M (NaCl) and 25 °C. [b] Bi-$H_3$tripa UV acidic spectrophotometric titration at 25 °C. [c] Pb-$H_3$tripa UV acidic spectrophotometric titration at 25 °C. Charges are omitted for clarity.

pM values are a useful parameter to compare chelators of different basicity and denticity for their metal scavenging ability, with higher pM values corresponding to stronger binding.[18] In Table S3† are listed the pM values of different macrocyclic chelators relevant in TAT. The pM data for $Pb^{2+}$ and $Bi^{3+}$ indicate that $H_3$tripa exhibits the highest binding affinity for both metal ions, with pBi = 30.2 and pPb = 25.1. In comparison, $H_4$DOTA shows the second highest pM values for $Pb^{2+}$, and retains high thermodynamic stability for $Bi^{3+}$.[19,20] A dipicolinate derivative of $H_4$DOTA, $H_2$Me-do2pa, demonstrates higher $Bi^{3+}$ affinity than $H_4$DOTA, confirming the strong binding preference of $Bi^{3+}$ for picolinates.[21] However, $H_2$Me-do2pa exhibits significantly lower affinity for $Pb^{2+}$. $H_2$macropa, containing two picolinic acid in a diaza-18-crown-6 ether backbone, shows lower affinity for $Pb^{2+}$ compared to $H_3$tripa[12] – possibly due to the different symmetry of the diaza-18-crown-6 framework and the absence of a third picolinic acid, which might allow for different arrangements around the $Pb^{2+}$. $H_2$BADPA-18, a benzene derivative of $H_2$macropa, exhibits strong $Bi^{3+}$ binding but reduced $Pb^{2+}$ affinity.[11] The lower affinity for $Pb^{2+}$ might be attributed to the increased conformational rigidity introduced by the benzene ring.

Lastly, we assessed the radiolabeling of $H_3$tripa with $[^{213}Bi]Bi^{3+}$ and $[^{203}Pb]Pb^{2+}$. Given the short half-life of $^{213}Bi$ (45.6 min), rapid radiolabeling kinetics (5–10 min) are essential to achieve near-complete incorporation of the radionuclide under mild conditions (ambient temperature, pH 5–7). The radiolabeling efficiency of $H_3$tripa for $[^{213}Bi]Bi^{3+}$ was evaluated across a range of ligand concentrations ($10^{-3}$–$10^{-7}$ M) at ambient temperature and compared to $H_4$DOTA at elevated temperature (80 °C) after a 10 minute incubation (Fig. 6A). $H_3$tripa demonstrated high efficiency, achieving quantitative incorporation of $[^{213}Bi]Bi^{3+}$ (>95% radiochemical conversion, RCC%) at $10^{-6}$ M, with a slight decrease to approximately 85%

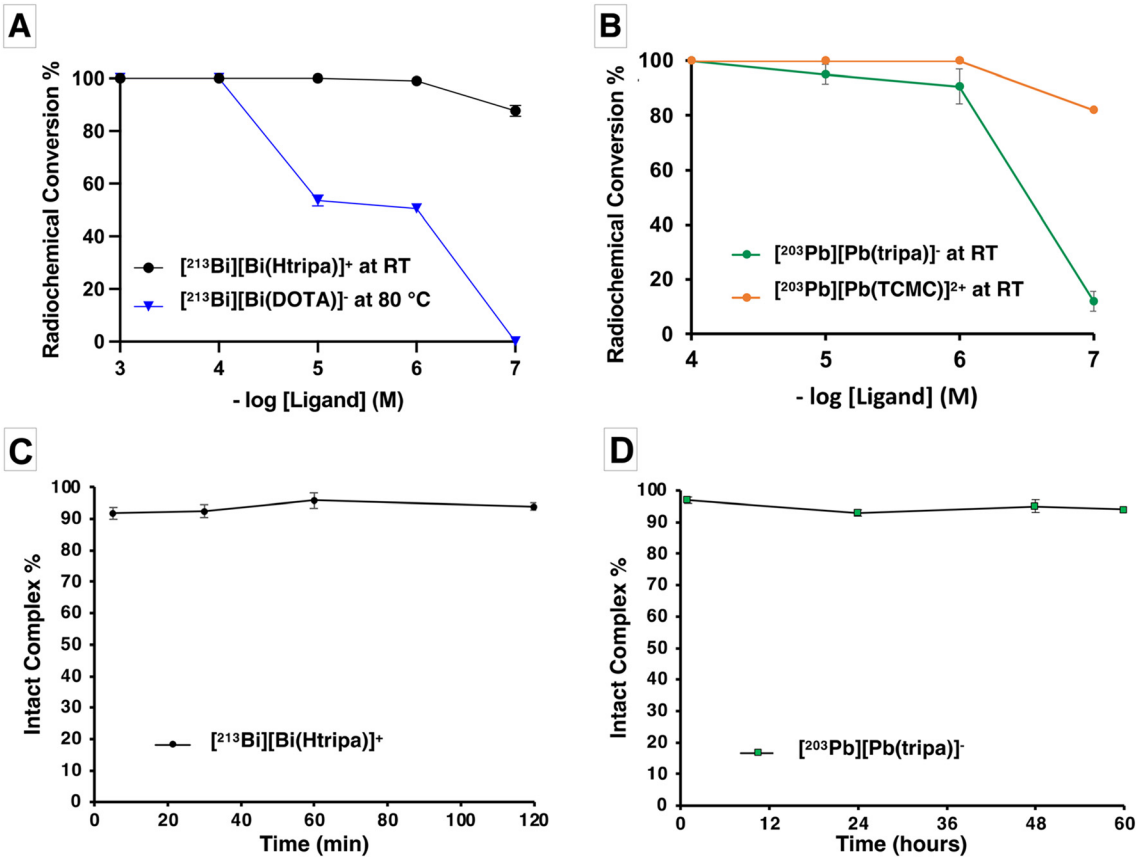


**Fig. 6** Concentration-dependent radiolabeling studies of $H_3$tripa and (A) DOTA with [$^{213}$Bi]$Bi^{3+}$(100 kBq) in MES (1 M, pH 5.5) and (B) TCMC with [$^{203}$Pb]$Pb^{2+}$(100 kBq) in $NH_4OAc$ (0.5 M, pH 7). Human serum stability studies of $H_3$tripa with (C) [$^{213}$Bi]$Bi^{3+}$ (200 kBq) and (D) [$^{203}$Pb]$Pb^{2+}$ (300 kBq). All reactions were performed at 37 °C and monitored using radio-TLC.

at $10^{-7}$ M. In contrast, $H_4$DOTA required a significantly higher concentration ($10^{-4}$ M) at 80 °C to achieve comparable radiolabeling efficiency. The performance of $H_3$tripa is comparable to that of $H_2$macropa and $H_2S_2$macropa[12] – all three chelators achieved quantitative chelation of [$^{213}$Bi]$Bi^{3+}$ down to $10^{-6}$ M, with RCC% dropping to ~80% at $10^{-7}$ M. $H_2$BADPA-18, tested with [$^{207}$Bi]$Bi^{3+}$ ($t_{1/2}$ = 31.2 years, EC), showed slightly lower yields compared to the other picolinic acid-based chelators.[11] This discrepancy may be partially attributed to the lower incubation time used for the $H_2$BADPA-18 radiolabeling (1–2 min).

Concentration-dependent radiolabeling studies with [$^{203}$Pb]$Pb^{2+}$ were conducted to evaluate the performance of $H_3$tripa compared to the gold-standard chelator for [$^{212/203}$Pb]$Pb^{2+}$, TCMC, at ambient temperature with a 30 minute incubation. $H_3$tripa achieved quantitative incorporation of [$^{203}$Pb]$Pb^{2+}$ at $10^{-5}$ M, with a slight decline to 91% at $10^{-6}$ M, while the RCC% decreased further at $10^{-7}$ M. In contrast, TCMC maintained higher radiolabeling efficiency at $10^{-7}$ M. Both $H_2S_2$macropa and $H_2$macropa were also capable of incorporating [$^{203}$Pb]$Pb^{2+}$ at $10^{-7}$ M, which deviates from the expected thermodynamic stability trends (pPb: $H_3$tripa > $H_2$macropa > $H_2S_2$macropa). This highlights the importance of radiolabeling studies over bulk solution stability assessments in the context of radiopharmaceutical development and translation.

The observed discrepancies may also be attributed to differences in experimental conditions, particularly the residual thallium present in the [$^{203}$Pb]$Pb^{2+}$ solution and the molarity of ammonium acetate ($NH_4OAc$) buffer used.[11] $H_3$tripa was radiolabeled in 0.5 M $NH_4OAc$, while $H_2S_2$macropa and $H_2$macropa were radiolabeled in 0.1 M $NH_4OAc$.[12] Since ammonium acetate can compete with the radiometal for chelator binding, the higher buffer concentration may have contributed to the reduced RCC% observed for $H_3$tripa.

The *in vitro* serum stability of both complexes was evaluated in human serum (Sigma-Aldrich H4522). [$^{213}$Bi][Bi(Htripa)]$^+$ was incubated for 2 hours (equivalent to approximately 2.6 half-lives of $^{213}$Bi), while [$^{203}$Pb][Pb(Htripa)] was incubated for 60 hours, with aliquots taken at specified time points (Fig. 6C and D). Both radiolabeled complexes demonstrated exceptional stability, remaining intact with over 95% radiochemical retention throughout their respective incubation periods. These results underscore the significant potential of $H_3$tripa as a chelator for radiopharmaceutical application.

## Conclusions

This work establishes $H_3$tripa as a versatile chelator for Pb/Bi theranostics, delivering rapid, high-yield radiolabeling of both isotopes at micromolar concentrations, and with exceptional human serum stability. Thermodynamic solution studies demonstrated, to our knowledge the highest stability constants reported to date for both $[Pb(tripa)]^-$ and Bi(tripa) complexes, underscoring the remarkable affinity of $H_3$tripa for these metals. NMR spectroscopy provided insights into the solution–state binding interactions, while X-ray crystallography of the $Pb^{2+}$ complex illustrated the binding preference of $H_3$tripa in the solid state. Additionally, DFT-optimized geometries indicated octadentate coordination for both metals, revealing that only two picolinic acid moieties contribute to strong interactions while the third may act more dynamically. Moving forward, efforts will focus on exploring structural modifications to incorporate a bifunctional handle, facilitating targeted, kit-style radiopharmaceutical development.

## Author contributions

Desiree Fiaccabrino: conceptualization, investigation, formal analysis, writing – original draft. Tinotenda Masvikeni: investigation, synthesis of precursors. Brooke McNeil: production of $[^{203}Pb]Pb^{2+}$. Brian O. Patrick: X-ray crystallography. María de Guadalupe Jaraquemada-Peláez: formal analysis, supervision, writing – review & editing. Paul Schaffer: funding acquisition, supervision, writing – review & editing. Chris Orvig: funding acquisition, supervision, writing – review & editing. All authors have given approval of the final version of the manuscript.

## Conflicts of interest

There are no conflicts to declare.

## Data availability

The data supporting this article have been included as part of the ESI.†

## Acknowledgements

Funding came from the Natural Sciences and Engineering Research Council (NSERC) of Canada through NSERC Discovery Grants (PS, CO). We gratefully acknowledge all personnel involved at TRIUMF's ISAC facility for ion beam delivery for $^{225}Ac$ production and Dr François Bénard at BC Cancer Research Institute for allowing the use of the Molecular Oncology laboratory to conduct experiments. TRIUMF receives federal funding *via* a contribution agreement with the National Research Council of Canada.

## References

1 P. M. D. Gape, M. K. Schultz, G. J. Stasiuk and S. Y. A. Terry, *Pharmaceuticals*, 2024, **17**, 334.
2 A. Morgenstern, C. Apostolidis, C. Kratochwil, M. Sathekge, L. Krolicki and F. Bruchertseifer, *Curr. Radiopharm.*, 2018, **11**, 200–208.
3 C. Kratochwil, K. Schmidt, A. Afshar-Oromieh, F. Bruchertseifer, H. Rathke, A. Morgenstern, U. Haberkorn and F. L. Giesel, *Eur. J. Nucl. Med. Mol. Imaging*, 2018, **45**, 31–37.
4 L. Wharton, C. Zhang, H. Yang, J. Zeisler, V. Radchenko, C. Rodríguez-Rodríguez, M. Osooly, B. O. Patrick, K.-S. Lin, F. Bénard, P. Schaffer and C. Orvig, *Bioconjugate Chem.*, 2022, **33**, 505–522.
5 J. De Swart, H. S. Chan, M. C. Goorden, A. Morgenstern, F. Bruchertseifer, F. J. Beekman, M. De Jong and M. W. Konijnenberg, *J. Nucl. Med.*, 2016, **57**, 486–492.
6 H. Zhu, S. Heinitz, K. Binnemans, S. Mullens and T. Cardinaels, *Inorg. Chem. Front.*, 2024, **11**, 4499–4527.
7 S. Mirzadeh, K. Kumar and O. A. Gansow, *Radiochim. Acta*, 1993, **60**, 1–10.
8 M. L. Grieve, P. R. W. J. Davey, P. V. Bernhardt, C. M. Forsyth and B. M. Paterson, *Inorg. Chem. Front.*, 2024, **11**, 7307–7323.
9 D. J. Fiszbein, V. Brown, N. A. Thiele, J. J. Woods, L. Wharton, S. N. MacMillan, V. Radchenko, C. F. Ramogida and J. J. Wilson, *Inorg. Chem.*, 2021, **60**, 9199–9211.
10 A. Hu, V. Brown, S. N. MacMillan, V. Radchenko, H. Yang, L. Wharton, C. F. Ramogida and J. J. Wilson, *Inorg. Chem.*, 2022, **61**, 801–806.
11 A. D. Zubenko, A. V. Pashanova, S. P. Mosaleva, E. Y. Chernikova, V. A. Karnoukhova, I. V. Fedyanin, B. V. Egorova, A. A. Shchukina, Y. V. Fedorov and O. A. Fedorova, *Inorg. Chem.*, 2024, **63**, 21652–21669.
12 P. Randhawa, K. J. Kadassery, B. L. McNeil, S. N. MacMillan, L. Wharton, H. Yang, J. J. Wilson and C. F. Ramogida, *Inorg. Chem.*, 2024, **63**, 21177–21193.
13 A. Hu, S. N. MacMillan and J. J. Wilson, *J. Am. Chem. Soc.*, 2020, **142**, 13500–13506.
14 A. Pellissier, Y. Bretonnière, N. Chatterton, J. Pécaut, P. Delangle and M. Mazzanti, *Inorg. Chem.*, 2007, **46**, 3714–3725.
15 G. Zampella, K. P. Neupane, L. De Gioia and V. L. Pecoraro, *Chem. – Eur. J.*, 2012, **18**, 2040–2050.
16 L. Shimoni-Livny, J. P. Glusker and C. W. Bock, *Inorg. Chem.*, 1998, **37**, 1853–1867.
17 A. Moncomble, J.-P. Cornard and M. Meyer, *J. Mol. Model*, 2017, **23**, 24.
18 W. R. Harris, C. J. Carrano and K. N. Raymond, *J. Am. Chem. Soc.*, 1979, **101**, 2213–2214.

 

19 M. Tosato, L. Lazzari and V. D. Marco, *ACS Omega*, 2022, **7**, 15596–15602.
20 É. Csajbók, Z. Baranyai, I. Bányai, E. Brücher, R. Király, A. Müller-Fahrnow, J. Platzek, B. Radüchel and M. Schäfer, *Inorg. Chem.*, 2003, **42**, 2342–2349.
21 L. M. P. Lima, M. Beyler, R. Delgado, C. Platas-Iglesias and R. Tripier, *Inorg. Chem.*, 2015, **54**, 7045–7057.
22 C. Orvig, CCDC 2448163: Experimental Crystal Structure Determination, 2025, DOI: **10.5517/ccdc.csd.cc2n5j0d**.